

Non-explosive hydrogen and helium burnings: Abundance predictions from the NACRE reaction rate compilation^{*}

M. Arnould, S. Goriely **, and A. Jorissen **

Institut d'Astronomie et d'Astrophysique, Université Libre de Bruxelles, CP 226, Boulevard du Triomphe, B-1050 Bruxelles, Belgium

19 January 1999; 19 April 1999

Abstract. The abundances of the isotopes of the elements from C to Al produced by the non-explosive CNO, NeNa and MgAl modes of hydrogen burning, as well as by helium burning, are calculated with the thermonuclear rates recommended by the European compilation of reaction rates for astrophysics (NACRE). The impact of nuclear physics uncertainties on the derived abundances is discussed in the framework of a simple parametric astrophysical model. These calculations have the virtue of being a guide in the selection of the nuclear uncertainties that have to be duly analyzed in detailed model stars, particularly in order to perform meaningful confrontations between abundance observations and predictions. They are also hoped to help nuclear astrophysicists pinpointing the rate uncertainties that have to be reduced most urgently.

Key words: Nuclear reactions – nucleosynthesis – abundances

1. Introduction

The evolution of a star is made of a succession of “controlled” thermonuclear burning stages interspersed with phases of gravitational contraction. The latter stages are responsible for a temperature increase, the former ones producing nuclear energy and composition changes.

As is well known, hydrogen and helium burning in the central regions or in peripheral layers of a star are key nuclear episodes, and leave clear observables, especially in the Hertzsprung-Russell diagram, or in the stellar surface composition. These photospheric abundance signatures may result from so-called “dredge-up” phases, which are expected to transport the H- or He-burning ashes from the deep production zones to the more external layers. This type of surface contamination is encountered especially in low- and intermediate-mass stars on their first

or asymptotic branches, where two to three dredge-up episodes have been identified by stellar evolution calculations. Nuclear burning ashes may also find their way to the surface of non-exploding stars by rotationally-induced mixing, which has been started to be investigated in some detail (Heger 1998), or by steady stellar winds, which have their most spectacular effects in massive stars of the Wolf-Rayet type.

The confrontation between the wealth of observed elemental or isotopic compositions and calculated abundances can provide essential clues on the stellar structure from the main sequence to the red giant phase, and much has indeed been written on this subject. Of course, the information one can extract from such a confrontation is most astrophysically useful if the discussion is freed from nuclear physics uncertainties to the largest possible extent.

Thanks to the impressive skill and dedication of some nuclear physicists, remarkable progress has been made over the years in our knowledge of reaction rates at energies which are as close as possible to those of astrophysical relevance (e.g. Rolfs & Rodney 1988). Despite these efforts, important uncertainties remain. This relates directly to the enormous problems the experiments have to face in this field, especially because the energies of astrophysical interest for charged-particle-induced reactions are much lower than the Coulomb barrier energies. As a consequence, the corresponding cross sections can dive into the nanobarn to picobarn abyss. In general, it has not been possible yet to measure directly such small cross sections. Theoreticians are thus requested to supply reliable extrapolations from the lowest energies attained experimentally to those of most direct astrophysical relevance.

Recently, a new major challenge has been taken up by a consortium of European laboratories with the build-up of well documented and evaluated sets of experimental data or theoretical predictions for a large number of astrophysically interesting nuclear reactions (Angulo et al. 1999). This compilation of reaction rates, referred to as NACRE (Nuclear Astrophysics Compilation of REaction rates; see Sect. 2 for some details), comprises in particular the rates for all the charged-particle-induced nuclear reactions involved in the “cold” pp-, CNO, NeNa and MgAl chains,

Send offprint requests to: S. Goriely

^{*} An electronic version of this paper, with colour figures, is available at <http://astro.ulb.ac.be>

^{**} Research Associate, F.N.R.S. (Belgium)

Correspondence to: sgoriely@astro.ulb.ac.be

the first two burning modes being essential energy producers, all four being important nucleosynthesis agents. It also includes the main reactions involved in non-explosive helium burning.

The aim of this paper is to calculate with the help of the NACRE data the abundances of the different isotopes of the elements from C to Al involved in the non-explosive H (Sects. 3 - 5) and He (Sect. 6) burnings, special emphasis being put on the impact of the reported remaining rate uncertainties on the derived abundances. The yields from the considered burning modes are calculated by combining in all possible ways the lower and upper limits of all the relevant reaction rates. One “reference” abundance calculation is also performed with all the recommended NACRE rates. Note that the pp-chains are not considered here. A solar neutrino analysis based on preliminary NACRE data for the pp reactions can be found in Castellani et al. (1997).

Our extensive abundance uncertainty analysis is performed in the framework of a parametric model assuming that H burning takes place at a constant density $\rho = 100 \text{ g cm}^{-3}$ and at constant temperatures between $T_6 = 10$ and 80 (T_n is the temperature in units of 10^n K). The corresponding typical values adopted for He burning are $\rho = 10^4 \text{ g cm}^{-3}$ and $T_8 = 1.5$ and 3.5. These ranges encompass typical burning conditions in a large variety of realistic stellar models. For the study of H-burning, initial abundances are assumed to be solar (Anders & Grevesse 1989). For He-burning, we adopt the abundances resulting from H burning at $T_6 = 60$ and $\rho = 100 \text{ g cm}^{-3}$ calculated with the use of the NACRE recommended rates. The H- and He-burning nucleosynthesis is followed until the H and He mass fractions drop to 10^{-5} .

In spite of its highly simplistic aspect, this analysis provides results that are of reasonable qualitative value, as testified by their confrontation with detailed stellar model predictions. Most significant, these parametric calculations have the virtue of identifying the rate uncertainties whose impact may be of significance on abundance predictions at temperatures of stellar relevance. They thus serve as a guide in the selection of the nuclear uncertainties that have to be duly analyzed in detailed model stars, particularly in order to perform meaningful confrontations between abundance observations and predictions. They are also hoped to help nuclear astrophysicists pinpointing the rate uncertainties that have to be reduced most urgently.

2. The NACRE compilation in a nutshell

A detailed information about the procedure adopted to evaluate each of the NACRE reaction rates and about the derived values can be found in Angulo et al. (1999), or in electronic form at <http://astro.ulb.ac.be>, which also offers the possibility of generating interactively tables of reaction rates for networks and temperature grids selected by the

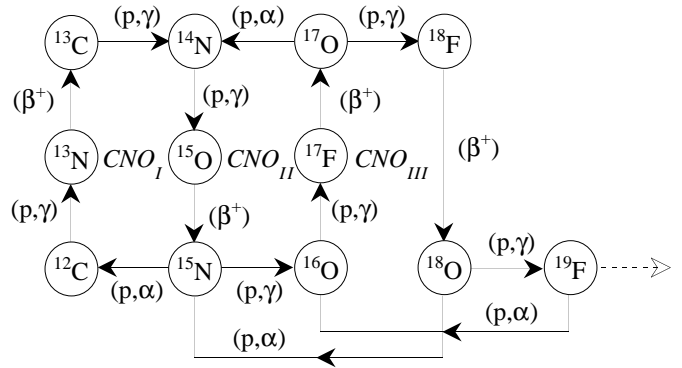


Fig. 1. Reactions of the CNO cycles. The dashed line represents the possible leakage out of the cycles

user¹. It is clearly impossible to go here into the details of the NACRE procedure. Let us just emphasize some of its specificities:

- (1) For each reaction, the non-resonant and broad-resonance contributions to its rate are evaluated numerically in order to avoid the approximations which are classically made (see Fowler et al. 1975 for details) in order to allow analytical rate evaluations;
- (2) Narrow or subthreshold resonances are in general approximated by Breit-Wigner shapes, and their contributions to the reaction rates are approximated in the usual analytical way (e.g. Fowler et al. 1975). However, in some cases, the resonance data are abundant enough to allow a numerical calculation avoiding these approximations;
- (3) For each reaction, NACRE provides a recommended “adopted” rate, along with realistic lower and upper limits. The adopted values of, and the limits on the resonance contributions are derived from weighted averages duly taking into account the uncertainties on individual measurements, as well as the different measurements that are sometimes available for a given resonance [see Eq. (15) of Angulo et al. 1999]. For non-resonant contributions, χ^2 -fits to available data provide the recommended values along with the lower and upper limits, as the experimental uncertainties on one set of data and the differences between various sets, if available, are taken into account in the χ^2 -procedure. It is worth stressing at this point that enough information is provided by NACRE for helping the user to tailor his own preferred rates if he wants.

The procedure just sketched in (1) - (3) is the selected standard methodology, and has the advantage of being easily reproducible and of avoiding any subjective renormalization of different experimental data sets. Quite clearly, however, the large variety of different situations makes unavoidable some slight modifications of the standard procedure in some cases. These specific adjustments are clearly identified and discussed in Angulo et al. (1999);

¹ This electronic address also provides many other nuclear data of nuclear astrophysics interest

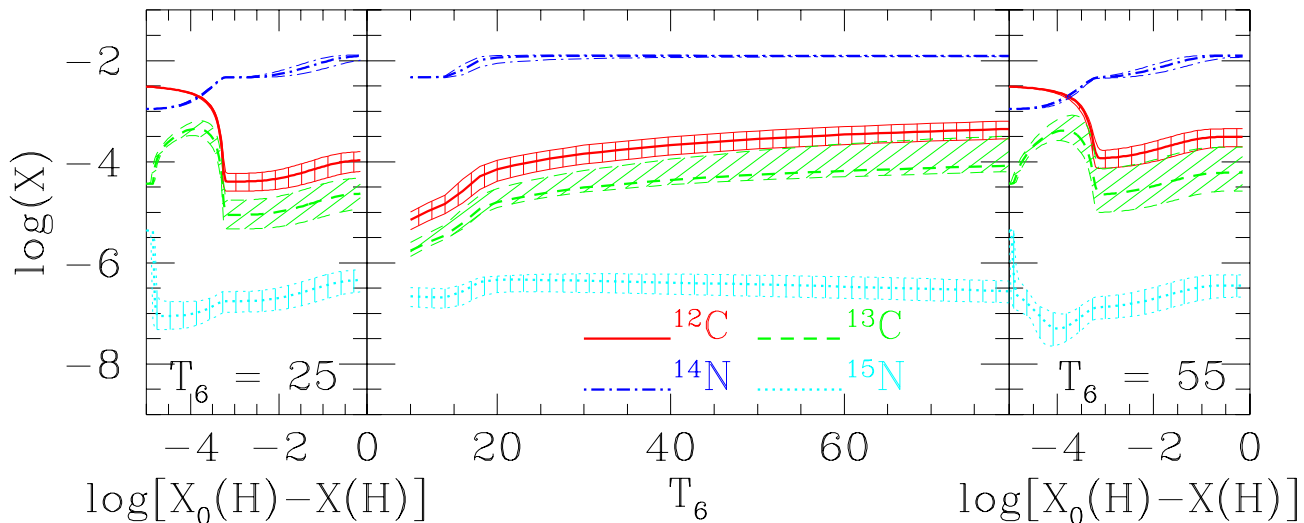


Fig. 2. *Left and right panels:* Time variations of the mass fractions of the stable C and N isotopes versus the amount of hydrogen burned at constant density $\rho = 100 \text{ g/cm}^3$ and constant temperatures $T_6 = 25$ and 55 . The H mass fraction is noted $X(\text{H})$, the subscript 0 corresponding to its initial value; *Middle panel:* Mass fractions of the same nuclides at H exhaustion [$X(\text{H})=10^{-5}$] as a function of T_6 . The shaded areas delineate the uncertainties resulting from the reaction rates

(4) A theoretical (Hauser-Feshbach) evaluation of the contribution to each rate of the thermally populated excited states of the target is also provided. It has to be noted that the widely used compilation of Caughlan & Fowler (1988, hereafter referred to as CF88) provides uncertainties for some rates only, while the contribution of excited target states is derived in most cases from a rough (referred to as “equal strength”) approximation;

(5) It has to be emphasized that the major goal of the NACRE compilation is to provide numerical reaction rates in tabular form (see <http://astro.ulb.ac.be>). This philosophy differs markedly from the one promoted by the previous widely used compilations (CF88, and references therein), and is expected to lead to more accurate rate data. However, for completeness, NACRE also provides analytical approximations (Angulo et al. 1999) that differ in several respects from the classically used expressions (CF88, and references therein).

3. The CNO Cycles

The reactions of the CNO cycles are displayed in Fig. 1. As is well known, their net result is the production of ${}^4\text{He}$ from H, and the transformation of the C, N and O isotopes mostly into ${}^{14}\text{N}$ as a result of the relative slowness of ${}^{14}\text{N}(p, \gamma){}^{15}\text{O}$ with respect to the other involved reactions. This ${}^{14}\text{N}$ build-up is clearly seen in Fig. 2.

As shown in Fig. 1, three nuclides are important branching points for the CNO cycles. The first one is ${}^{15}\text{N}$. At $T_6 = 25$, ${}^{15}\text{N}(p, \alpha){}^{12}\text{C}$ is 1000 times faster than

${}^{15}\text{N}(p, \gamma){}^{16}\text{O}$, and the CN cycle reaches equilibrium already before 10^{-3} of the initial protons have been burned. The second branching is at ${}^{17}\text{O}$. The competing reactions ${}^{17}\text{O}(p, \alpha){}^{14}\text{N}$ and ${}^{17}\text{O}(p, \gamma){}^{18}\text{F}$ determine the relative importance of cycle II over cycle III (Fig. 1). The uncertainties on these rates have been strongly reduced in the last years. The rate of ${}^{17}\text{O}(p, \alpha){}^{14}\text{N}$ recommended by NACRE is larger than the CF88 one by factors of 13 and 90 at $T_6 = 20$ and 80 , respectively. Smaller deviations, though reaching a factor of 9 at $T_6 = 50$, are found for the ${}^{17}\text{O}(p, \gamma){}^{18}\text{F}$ rate.

The oxygen isotopic composition is shown in Fig. 3. As it is well known, it depends drastically on the burning temperature. In particular, ${}^{17}\text{O}$ is produced at $T_6 \lesssim 25$, but is destroyed at higher temperatures. This has the important consequence that the amount of ${}^{17}\text{O}$ emerging from the CNO cycles and eventually transported to the stellar surface is a steep function of the stellar mass. This conclusion could get some support from the observation of a large spread in the oxygen isotopic ratios at the surface of red giant stars of somewhat different masses (Dearborn 1992, and references therein). Fig. 3 also demonstrates that the oxygen isotopic composition cannot be fully reliably predicted yet at a given temperature as a result of the cumulative uncertainties associated with the different production and destruction rates.

Finally, the leakage from cycle III is determined by the ratio of the ${}^{18}\text{O}(p, \gamma){}^{19}\text{F}$ and ${}^{18}\text{O}(p, \alpha){}^{15}\text{N}$ rates (Fig. 1). At the temperatures of relevance, ${}^{18}\text{O}(p, \gamma){}^{19}\text{F}$ is roughly 1000 times slower than ${}^{18}\text{O}(p, \alpha){}^{15}\text{N}$, in rel-

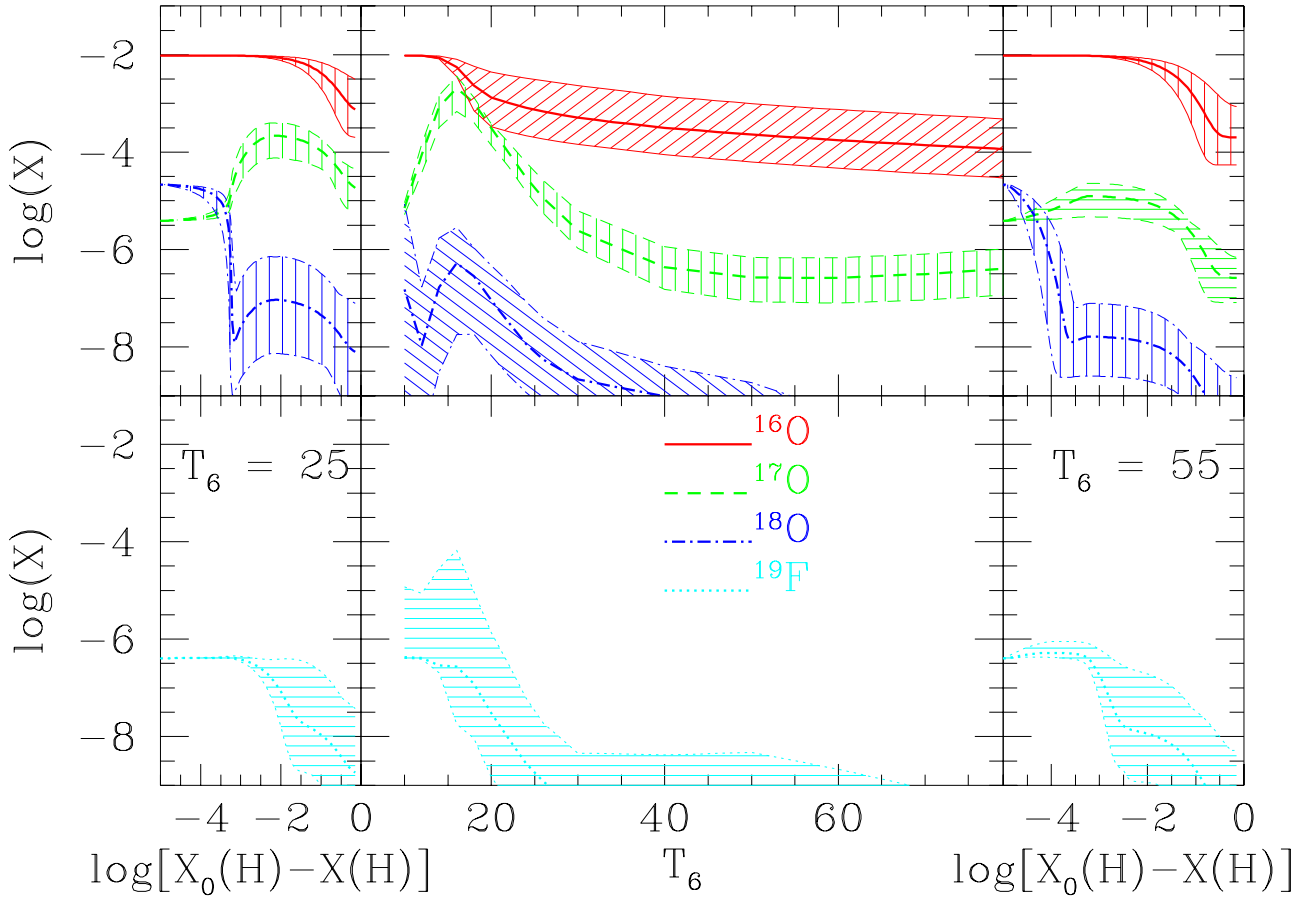


Fig. 3. Same as Fig. 2, but for the O and F nuclides

atively good agreement with CF88 (Fig. 4), undermining the path leading to the production of ^{19}F . However, at low temperatures, large uncertainties still affect the $^{18}\text{O}(p, \gamma)^{19}\text{F}$ rate. In fact, its upper bound could be comparable to the $^{18}\text{O}(p, \alpha)^{15}\text{N}$ rate, and at the same time larger than the $^{19}\text{F}(p, \alpha)^{16}\text{O}$ rate at $T_6 \lesssim 20$. As a result, some ^{19}F might be produced, in contradiction with the conclusion drawn from the adoption of the CF88 rates. Fig. 3 indeed confirms that fluorine could be overproduced (with respect to solar) by up to a factor of 100 at H exhaustion when $T_6 \approx 15$. However, Fig. 3 also reveals that the maximum ^{19}F yields that can be attained remain very poorly predictable as a result of the rate uncertainties. In fact, some hint of a non-negligible production of fluorine by the CNO cycles might come from the observation of fluorine abundances slightly larger than solar at the surface of red giant stars considered to be in their post-first dredge-up phase (Jorissen et al. 1992; Mowlavi et al. 1996).

As far as $^{18}\text{O}(p, \alpha)^{15}\text{N}$ is concerned, let us also mention that Huss et al. (1997) have speculated that its rate could be about 1000 times larger than the one adopted by CF88 and NACRE at temperatures of about 15×10^6 K.

This proposal has been made in order to explain the N isotopic composition measured in some presolar grains. It is clearly fully incompatible with the NACRE analysis.

Finally, let us note that $^{19}\text{F}(p, \alpha)^{16}\text{O}$ is always much faster than $^{19}\text{F}(p, \gamma)^{20}\text{Ne}$. Any important leakage out of the CNO cycles to ^{20}Ne is thus prevented, this conclusion being independent of the remaining rate uncertainties.

4. The NeNa Chain

The NeNa chain is illustrated in Fig. 5, while Fig. 6 displays some relevant NACRE reaction rates, and their, sometimes quite large, uncertainties. These affect in particular the proton captures by ^{21}Ne , ^{22}Ne and ^{23}Na . In contrast, the $^{20}\text{Ne}(p, \gamma)^{21}\text{Na}$ rate may be considered as relatively well determined. Some of these rates may also deviate strongly from the CF88 proposed values.

The NACRE rates are used to compute the abundances shown in Fig. 7. A slight alteration of the initial ^{20}Ne abundance is visible only for $T_6 \gtrsim 50$. However, an unnoticeable ^{20}Ne destruction is sufficient to lead to a significant increase of the abundance of the rare ^{21}Ne iso-

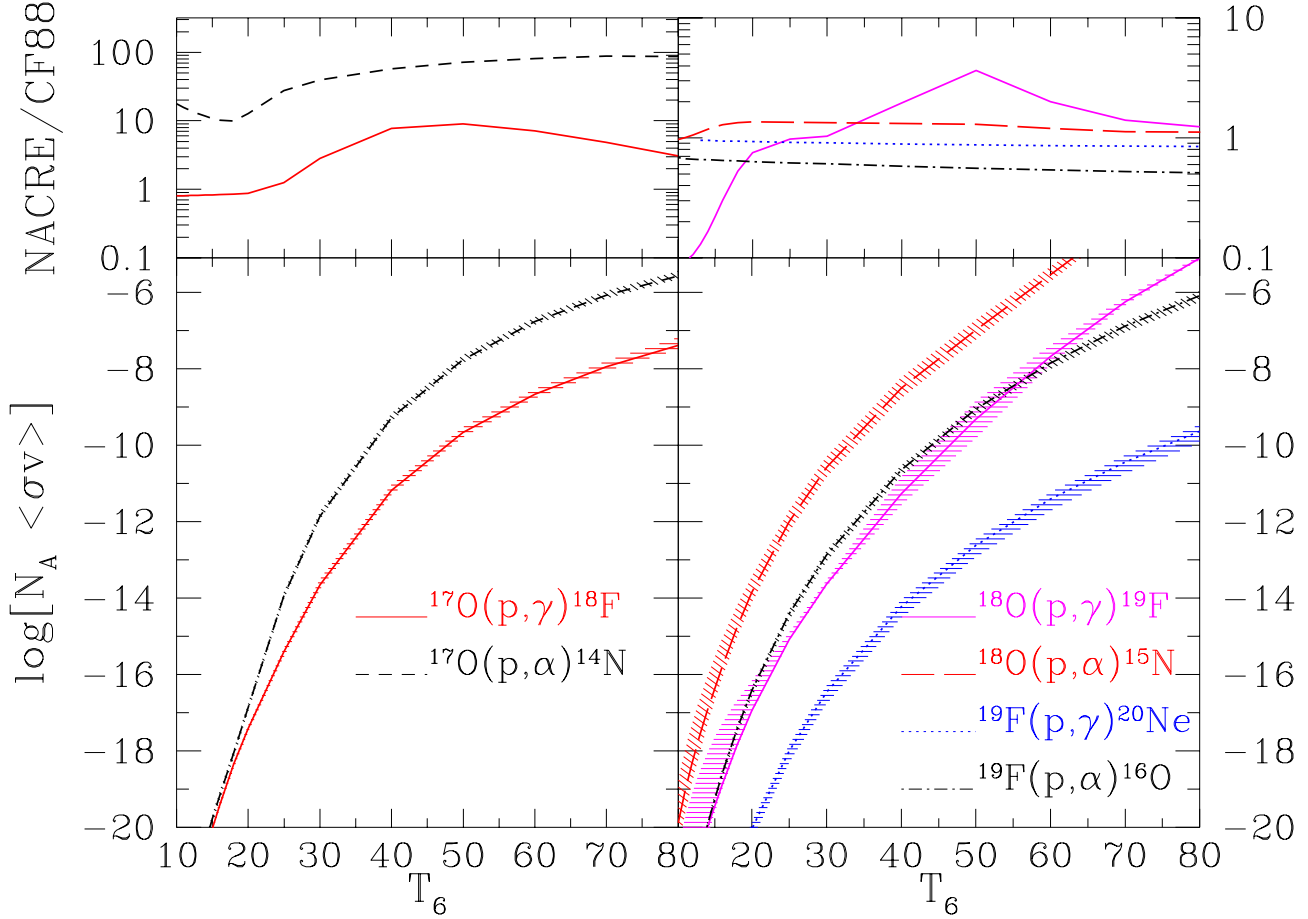


Fig. 4. Bottom panels: Temperature dependence of Maxwellian-averaged reaction rates (expressed in $\text{cm}^3 \text{mol}^{-1} \text{s}^{-1}$) from NACRE for proton capture by ^{17}O (left panel) and by ^{18}O and ^{19}F (right panel). The rate uncertainties given by NACRE are represented by the shaded area. Top panels: Ratio between the NACRE and CF88 Maxwellian-averaged reaction rates

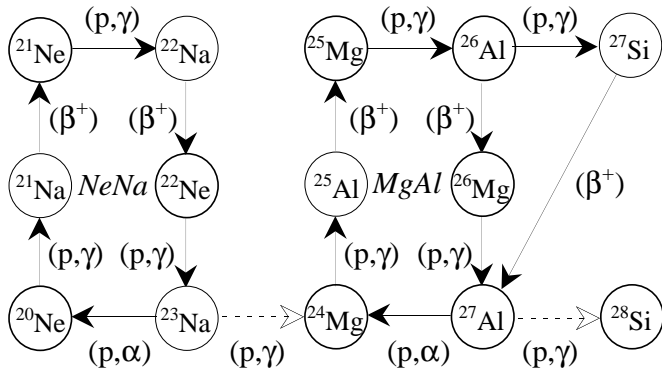


Fig. 5. Same as Fig. 1, but for the NeNa and MgAl chains

tope through $^{20}\text{Ne}(p, \gamma)^{21}\text{Na}(\beta^+)^{21}\text{Ne}$ at $T_6 \lesssim 40$. At higher temperatures, $^{21}\text{Ne}(p, \gamma)^{22}\text{Na}(\beta^+)^{22}\text{Ne}$ destroys ^{21}Ne . As a result, the ^{21}Ne abundance at H exhaustion is maximum when H burns in the approximate $30 \lesssim T_6 \lesssim 35$

range. This conclusion may, however, be altered if the upper limit of the $^{21}\text{Ne}(p, \gamma)^{22}\text{Na}$ rate is adopted instead.

The ^{23}Na yield has raised much interest recently, following the discovery at the surface of globular cluster red giant stars of moderate sodium overabundances which correlate or anti-correlate with the amount of other elements (like C, N, O, Mg and Al) also involved in cold H burning (Denissenkov et al. 1998; Kraft et al. 1998, and references therein). This situation may be the signature of the dredge-up to the stellar surface of the ashes of the NeNa chain. The ^{23}Na production results from $^{22}\text{Ne}(p, \gamma)^{23}\text{Na}$, while $^{23}\text{Na}(p, \gamma)^{24}\text{Mg}$ and $^{23}\text{Na}(p, \alpha)^{20}\text{Ne}$ are responsible for its destruction, which can be substantial at $T_6 \gtrsim 60$. Unfortunately, our knowledge of these three reaction rates remains very poor, with uncertainties that can amount to factors of about 100 to 10^4 in certain temperature ranges (see Fig. 6). As indicated in Fig. 7, this situation prevents an accurate prediction of the ^{23}Na yields when $T_6 \gtrsim 50$. More precisely, the spread in the

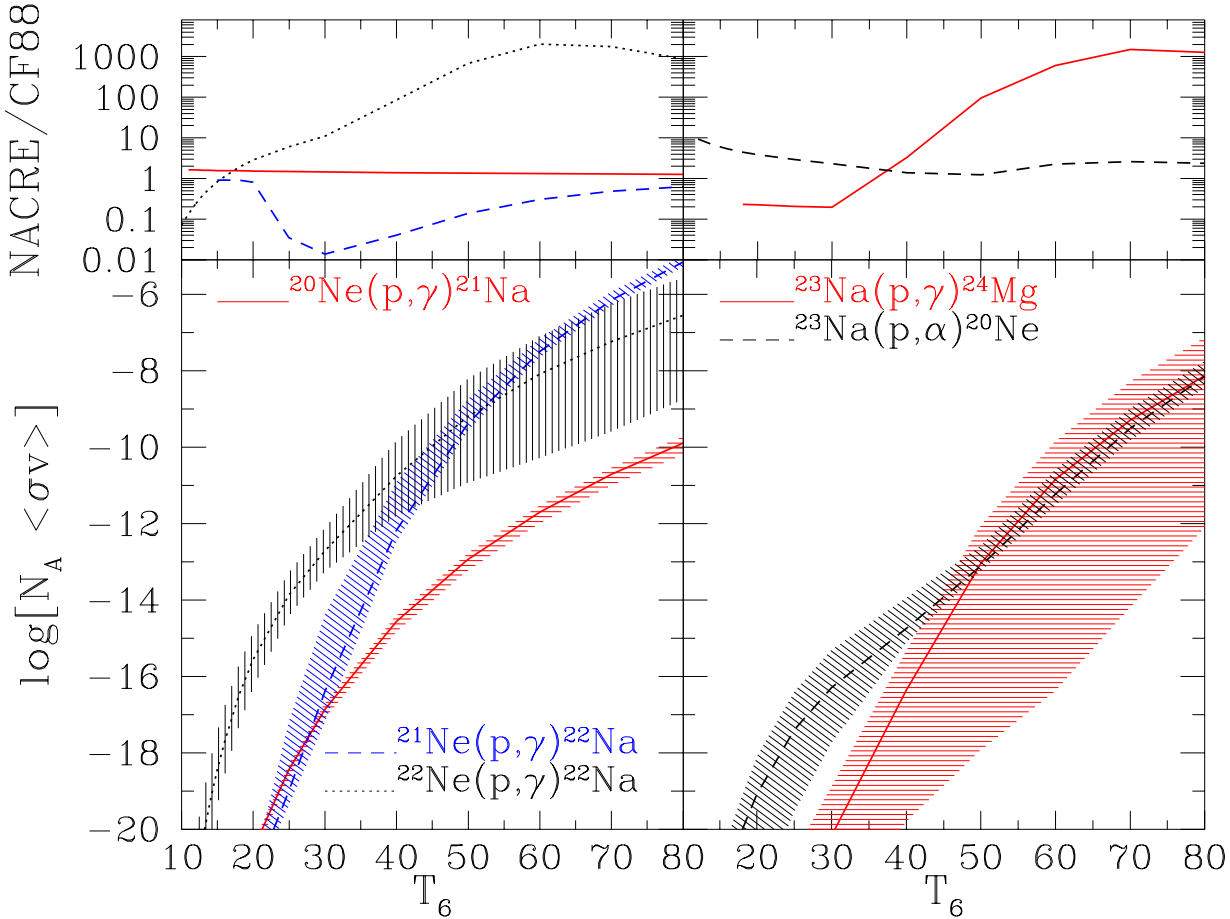


Fig. 6. Same as Fig. 4, but for $^{20}\text{Ne}(p,\gamma)^{21}\text{Na}$, $^{21}\text{Ne}(p,\gamma)^{22}\text{Na}$, $^{22}\text{Ne}(p,\gamma)^{23}\text{Na}$ (left panel) and $^{23}\text{Na}(p,\gamma)^{24}\text{Mg}$, $^{23}\text{Na}(p,\alpha)^{20}\text{Ne}$ (right panel)

^{23}Na abundance at H exhaustion reaches a factor of 100 at these temperatures.

The possible cycling character of the NeNa chain is determined by the ratio of the rates of $^{23}\text{Na}(p,\alpha)^{20}\text{Ne}$ and of $^{23}\text{Na}(p,\gamma)^{24}\text{Mg}$. Fig. 6 indicates that the former reaction is predicted to be faster than the latter one at $T_6 \lesssim 50$ only. In this case, the NeNa chain is indeed a cycle. However, at higher temperatures, an important leakage to the MgAl chain can be expected, unless future experiments confirm the lower bound of the uncertain $^{23}\text{Na}(p,\gamma)^{24}\text{Mg}$ rate.

5. The MgAl Chain

The MgAl chain is depicted in Fig. 5. It involves in particular ^{26}Al . Its long-lived ($t_{1/2} = 7.05 \times 10^5$ y) $^{26}\text{Al}^g$ ground state and its short-lived ($t_{1/2} = 6.35$ s) $^{26}\text{Al}^m$ isomeric state are out of thermal equilibrium at the temperatures of relevance for the non-explosive burning of hydrogen (Coc & Porquet 1998). They have thus to be considered as separate species in abundance calculations.

The status of our present knowledge of some important reactions of the MgAl chain is depicted in Fig. 8, while the yield predictions for the species involved in this chain are presented in Fig. 9. Let us first discuss the situation resulting from the use of the NACRE adopted rates. The most abundant nuclide is ^{24}Mg , the concentration of which remains unaffected, at least for $T_6 \lesssim 60$. In contrast, ^{25}Mg is significantly transformed by proton captures into $^{26}\text{Al}^g$ at $T_6 \gtrsim 30$. At $T_6 \gtrsim 50$, the leakage from the NeNa cycle starts affecting the MgAl nucleosynthesis through a slight increase of the ^{24}Mg abundance, followed by a modest enhancement of the ^{25}Mg , $^{26}\text{Al}^g$ and ^{27}Al concentrations (Fig. 9). At temperatures $T_6 \gtrsim 70$, the ^{24}Mg accumulation starts turning into a depletion by proton captures, which contributes to a further increase in the ^{25}Mg , $^{26}\text{Al}^g$ and ^{27}Al abundances. This build-up cannot be significantly hampered by the destruction of these species by proton captures, as a result of their relative slowness. Among these reactions, $^{27}\text{Al}(p,\alpha)^{24}\text{Mg}$ and $^{27}\text{Al}(p,\gamma)^{28}\text{Si}$ are of special interest, as the ratio of their rates determines in particular the leakage out of the

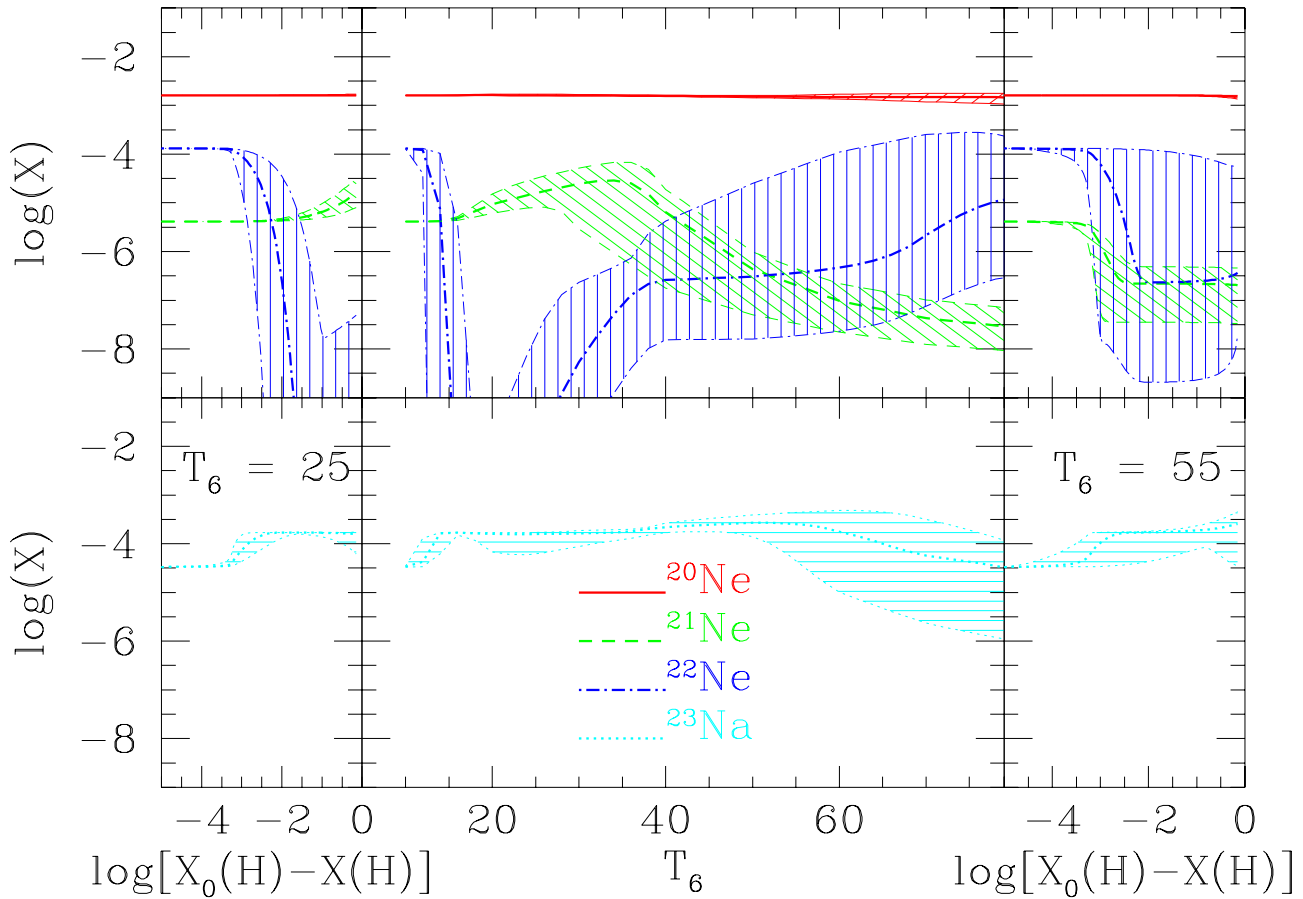


Fig. 7. Same as Fig. 2, but for the nuclides involved in the NeNa chain

MgAl chain. The adopted NACRE rate of the former reaction is 20 to 100 times slower than the CF88 one in the considered temperature range, and turns out to be slower than the (p, γ) channel for $T_6 \gtrsim 60$ (Fig. 8), so that no cycling back is possible in these conditions.

It is noticeable that the ^{26}Mg abundance at H exhaustion is almost temperature independent. This trend differs from the behaviour of the concentrations of the other Mg and Al isotopes, and results from two factors. First, the adopted ^{26}Mg proton capture is slow enough (about ten times slower than prescribed by CF88) for preventing ^{26}Mg to be destroyed at the considered temperatures. Second, ^{26}Mg is bypassed by the nuclear flow associated with the leakage from the NeNa chain at $T_6 \gtrsim 50$. The reaction $^{26}\text{Al}^g(p, \gamma)^{27}\text{Al}$ is indeed predicted to be faster than the $^{26}\text{Al}^g$ β -decay in this temperature domain.

Various aspects of the above analysis may be affected by remaining rate uncertainties. In fact, the only proton captures whose rates are now put on safe grounds are $^{24}\text{Mg}(p, \gamma)^{25}\text{Al}$ (for which NACRE and CF88 are in good agreement) and $^{25}\text{Mg}(p, \gamma)^{26}\text{Al}$ (for which the NACRE adopted rate is about 5 times slower than the CF88 one at

$T_6 < 80$). In spite of much recent effort, the other proton capture rates of the MgAl chain still show more or less large uncertainties in the considered temperature range, as illustrated in Fig. 8.

Due consideration of these uncertainties indicates in particular (see Fig. 9) that, for $T_6 \gtrsim 50$, ^{24}Mg could be more strongly destroyed than stated above, while ^{26}Mg could be substantially transformed into ^{27}Al if the NACRE upper limits on the $^{24}\text{Mg}(p, \gamma)^{25}\text{Al}$ and $^{26}\text{Mg}(p, \gamma)^{27}\text{Al}$ rates were selected. It is also important to note that the abundances at H exhaustion of $^{26}\text{Al}^g$ and ^{27}Al are not drastically affected by the uncertainties left in their proton capture rates, even if these uncertainties can be quite large (for example, the $^{26}\text{Al}^g(p, \gamma)^{27}\text{Si}$ rate is uncertain by more than a factor of 10^3 at $T_6 \gtrsim 50$). This situation results from the fact that even the highest NACRE proton capture rates are not fast enough for leading to a substantial destruction of the two Al isotopes

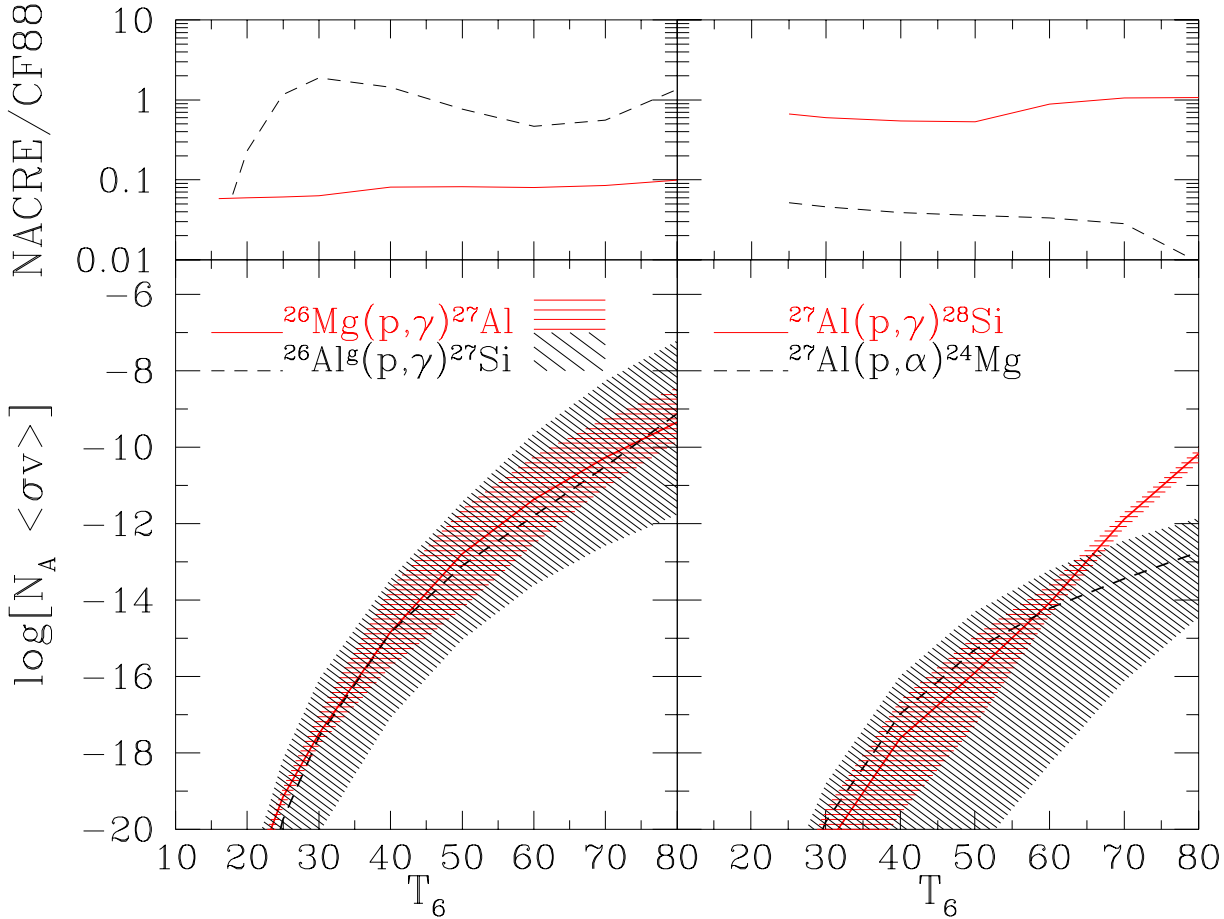


Fig. 8. Same as Fig. 4, but for $^{26}\text{Mg}(p, \gamma)^{27}\text{Al}$, $^{26}\text{Al}^g(p, \gamma)^{27}\text{Al}$ (left panel) and $^{27}\text{Al}(p, \gamma)^{28}\text{Si}$, $^{27}\text{Al}(p, \alpha)^{24}\text{Mg}$ (right panel)

by the time H is consumed². In contrast, the exact conditions under which the MgAl chain is cycling cannot be reliably specified yet in view of the large uncertainties still affecting the $^{27}\text{Al}(p, \alpha)^{24}\text{Mg}$ and $^{27}\text{Al}(p, \gamma)^{28}\text{Si}$ rates.

The possibility for the MgAl chain to produce substantial amounts of $^{26}\text{Al}^g$ is of high interest in view of the prime importance of this radionuclide in cosmochemistry and γ -ray line astronomy. There is now ample observational evidence that ^{26}Al has been injected live in the forming solar system before its in situ decay in various meteoritic inclusions (MacPherson et al. 1995). Its presence in extinct form is also demonstrated in various types of presolar grains of supposedly circumstellar origin identified in primitive meteorites (e.g. Zinner 1995). The present-day galactic plane also contains $^{26}\text{Al}^g$, as shown by the observation of a 1.8 MeV γ -ray line associated with its β -decay (e.g. Prantzos & Diehl 1996).

² Arnould et al. (1995) have reached a different conclusion due to a trivial mistake in the $^{26}\text{Al}^g(p, \gamma)^{27}\text{Si}$ rate used in their calculations

The MgAl chain has also a direct bearing on the puzzling Mg-Al anticorrelation observed in globular cluster red giants. Denissenkov et al. (1998) have speculated that a strong low-energy resonance could dominate the rate of $^{24}\text{Mg}(p, \gamma)^{25}\text{Al}$ at typical cold H-burning temperatures, and could help explaining these observations. There is at present no support of any sort to such a resonant enhancement of this rate.

6. Helium burning

The NACRE compilation also provides recommended rates and their lower and upper limits for most of the α -captures involved in the non-explosive burning of helium. The impact of the remaining rate uncertainties on the abundances of the elements up to Al affected by He burning is evaluated in our parametric model for two sets of conditions: (i) $\rho = 10^4 \text{ g cm}^{-3}$ and $T_8 = 1.5$, adopted to characterize the central or shell He-burning phases of intermediate-mass stars ($M \simeq 6 M_\odot$), and (ii) $\rho = 10^4 \text{ g cm}^{-3}$ and $T_8 = 3.5$, which can be encoun-

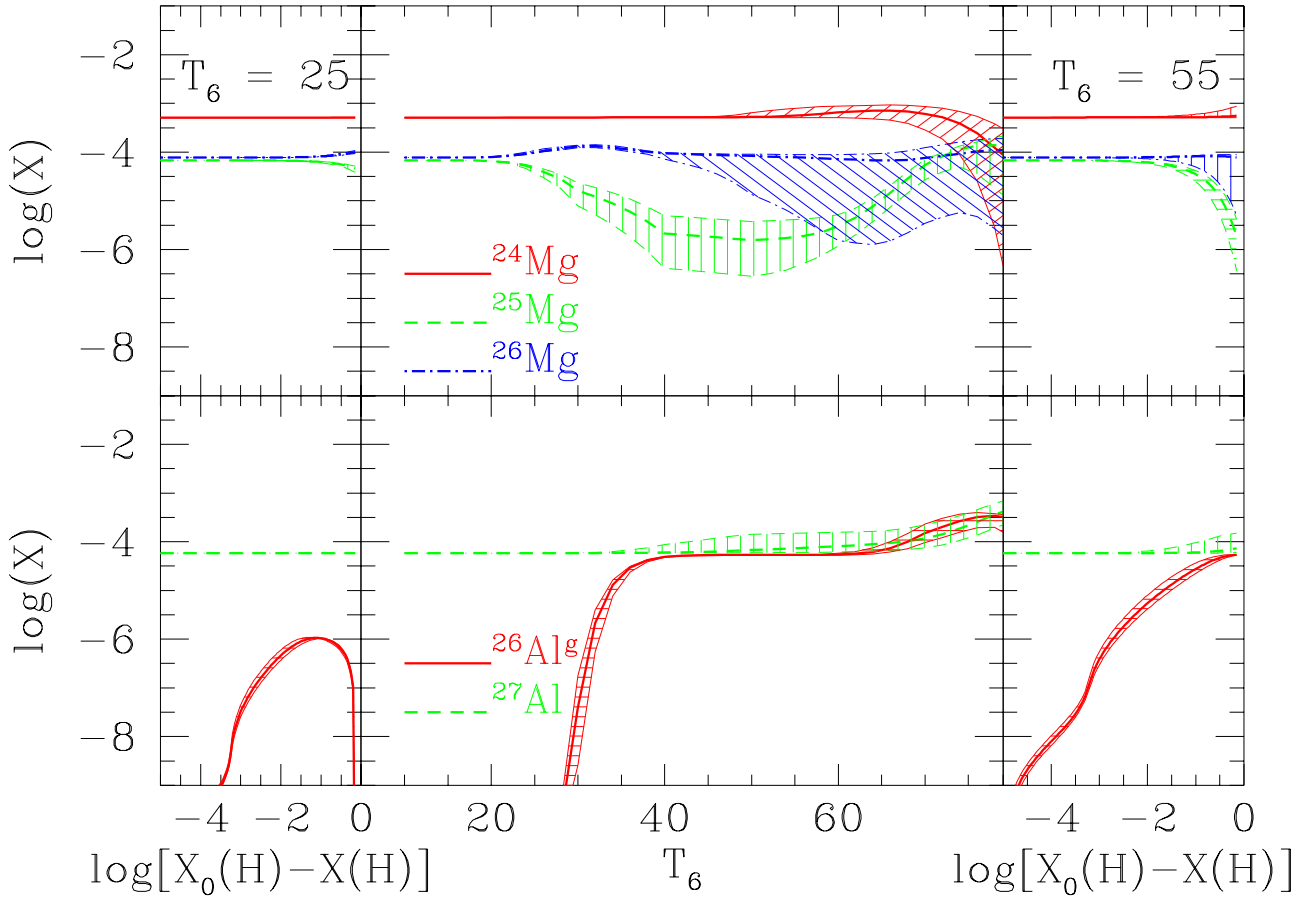


Fig. 9. Same as Fig. 2, but for the nuclides involved in the MgAl chain

tered at the end of the He burning phase in the core of massive stars or in AGB thermal pulses. The initial abundances used in these calculations are adopted as described in Sect. 1.

In contrast to the H-burning case, the abundances during He burning exhibit some sensitivity to density, as it enters differently the 3α reaction rate and the other α -capture rates. Consequently, the results presented here should not be used to infer abundances resulting from He burning in specific stellar models, where the time evolution of the temperature and the density may play an important role on the final He-burning composition. It has also to be noted that the neutrons produced by $^{13}\text{C}(\alpha, n)^{16}\text{O}$ or $^{22}\text{Ne}(\alpha, n)^{25}\text{Mg}$ during He burning lead us to extend the nuclear network to all (about 500) the s-process nuclides up to Bi.

Figs. 10 and 11 illustrate the evolution during He burning in the two situations mentioned above of the abundances of all the stable nuclides between ^{12}C and ^{27}Al (plus ^{26}Al). At low temperature ($T_8 \approx 1.5$; Figs. 10a and 11a), the main reaction flows are

a) $2\alpha(\alpha, \gamma)^{12}\text{C}$, followed by $^{12}\text{C}(\alpha, \gamma)^{16}\text{O}$ at the very end of He burning. The factor of 2 uncertainty in the rate of $^{12}\text{C}(\alpha, \gamma)^{16}\text{O}$ (Fig. 12) is responsible for the error bars on the ^{16}O abundance;

b) $^{14}\text{N}(\alpha, \gamma)^{18}\text{F}(\beta^+)^{18}\text{O}$, followed by $^{18}\text{O}(\alpha, \gamma)^{22}\text{Ne}$ at the end of He burning. The resulting ^{22}Ne does not burn at the considered low temperature³. The uncertainties of a factor of 1.5 and 5 at $T_8 = 1.5$ in the NACRE rates of $^{14}\text{N}(\alpha, \gamma)^{18}\text{F}$ and $^{18}\text{O}(\alpha, \gamma)^{22}\text{Ne}$, respectively (Fig. 12), are responsible for the wide range of predicted ^{18}O and ^{22}Ne abundances. A much larger ^{18}O abundance at the end of He burning would result if use were made of the CF88 rate, which is about 220 times smaller than the NACRE one (Fig. 12).

The neutron density resulting from $^{13}\text{C}(\alpha, n)^{16}\text{O}$ is shown in Fig. 13, along with its associated uncertainty. Albeit small, this neutron irradiation is responsible for the

³ In detailed stellar models, the temperature increases to values in excess of $T_8 = 3$ towards the end of core (or shell) He-burning. This may lead to the destruction of ^{22}Ne by (α, n) (with a concomitant production of neutrons) or (α, γ) reactions, as illustrated on Fig. 11b

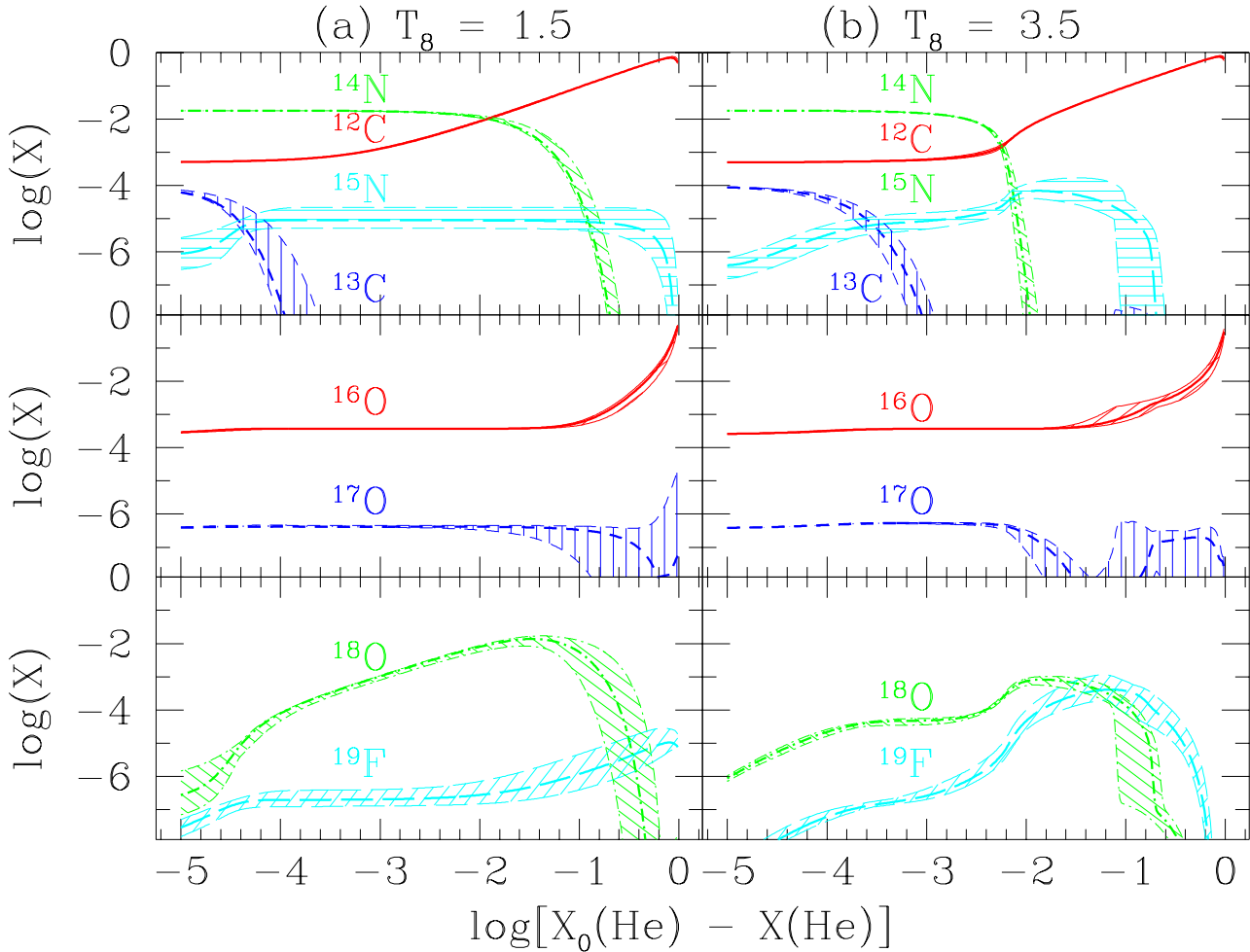


Fig. 10. Mass fractions of the stable C to F isotopes versus the amount of ${}^4\text{He}$ burned at constant density $\rho = 10^4 \text{ g/cm}^3$ and constant temperature $T_8 = 1.5$ (a: left panel) or $T_8 = 3.5$ (b: right panel). The ${}^4\text{He}$ mass fraction is denoted $X(\text{He})$, the subscript 0 corresponding to its initial value

${}^{15}\text{N}$ and ${}^{19}\text{F}$ abundance peaks seen in Fig. 10a. They result from ${}^{14}\text{N}(\alpha, \gamma){}^{18}\text{F}(\beta^+){}^{18}\text{O}(\text{p}, \alpha){}^{15}\text{N}(\alpha, \gamma){}^{19}\text{F}$, the protons originating from ${}^{14}\text{N}(\text{n}, \text{p}){}^{14}\text{C}$. Towards the end of He burning, ${}^{19}\text{F}$ is destroyed by ${}^{19}\text{F}(\alpha, \text{p}){}^{22}\text{Ne}$. Shell He burning in AGB stars or central He burning in Wolf-Rayet stars have been proposed as a major site for the galactic production of ${}^{19}\text{F}$ (Goriely et al. 1989; Meynet & Arnould 1996, 1999; Mowlavi et al. 1998). For AGB stars, these predictions have been confirmed by the observation of ${}^{19}\text{F}$ overabundances in some of these objects (Jorissen et al. 1992). Incomplete He-burning (e.g. in Wolf-Rayet stars) may also contribute to the galactic enrichment in primary ${}^{15}\text{N}$, as required by the observations of this nuclide in the interstellar medium (Güsten & Ungerechts 1985).

The large ${}^{26}\text{Al}$ abundance seen on Fig. 11a results from the particular choice of initial conditions (see Sect. 1), since ${}^{26}\text{Al}$ is not produced in the conditions prevailing during He-burning. Its rapid drop close to the end of He burning results from the combined effect of β -decay and

${}^{26}\text{Al}(\text{n}, \text{p}){}^{26}\text{Mg}$ making use of the few neutrons liberated by ${}^{22}\text{Ne}(\alpha, \text{n}){}^{25}\text{Mg}$.

At higher temperatures (Figs. 10b and 11b), the He-burning nucleosynthesis of the elements up to about Al is essentially the same as in the low temperature case. The major differences are observed for ${}^{18}\text{O}$, ${}^{19}\text{F}$, ${}^{21}\text{Ne}$, ${}^{22}\text{Ne}$, ${}^{25}\text{Mg}$, ${}^{26}\text{Mg}$ and ${}^{26}\text{Al}$, and are mainly due to a larger neutron production by ${}^{13}\text{C}(\alpha, \text{n}){}^{16}\text{O}$, ${}^{18}\text{O}(\alpha, \text{n}){}^{21}\text{Ne}$ and ${}^{22}\text{Ne}(\alpha, \text{n}){}^{25}\text{Mg}$. Note that ${}^{18}\text{O}(\alpha, \text{n}){}^{21}\text{Ne}$ is about 150 times slower than ${}^{18}\text{O}(\alpha, \gamma){}^{22}\text{Ne}$ in these conditions, but is fast enough to keep the neutron density above $N_n = 10^9 \text{ cm}^{-3}$ (Fig. 13). These neutrons allow protons to be produced by the reactions ${}^{14}\text{N}(\text{n}, \text{p}){}^{14}\text{C}$ and ${}^{18}\text{F}(\text{n}, \text{p}){}^{18}\text{O}$. Additional protons come from ${}^{18}\text{F}(\alpha, \text{p}){}^{21}\text{Ne}$. As a result, ${}^{15}\text{N}$ is produced via ${}^{18}\text{F}(\text{n}, \alpha){}^{15}\text{N}$, ${}^{18}\text{O}(\text{p}, \alpha){}^{15}\text{N}$, ${}^{14}\text{N}(\text{p}, \gamma){}^{15}\text{O}(\beta^+){}^{15}\text{N}$ and ${}^{18}\text{F}(\text{p}, \alpha){}^{15}\text{O}(\beta^+){}^{15}\text{N}$. The production of ${}^{19}\text{F}$ follows from ${}^{15}\text{N}(\alpha, \gamma){}^{19}\text{F}$. Since most of the involved reactions have better known rates at $T_8 = 3.5$ than at $T_8 = 1.5$, the corresponding error bars on the

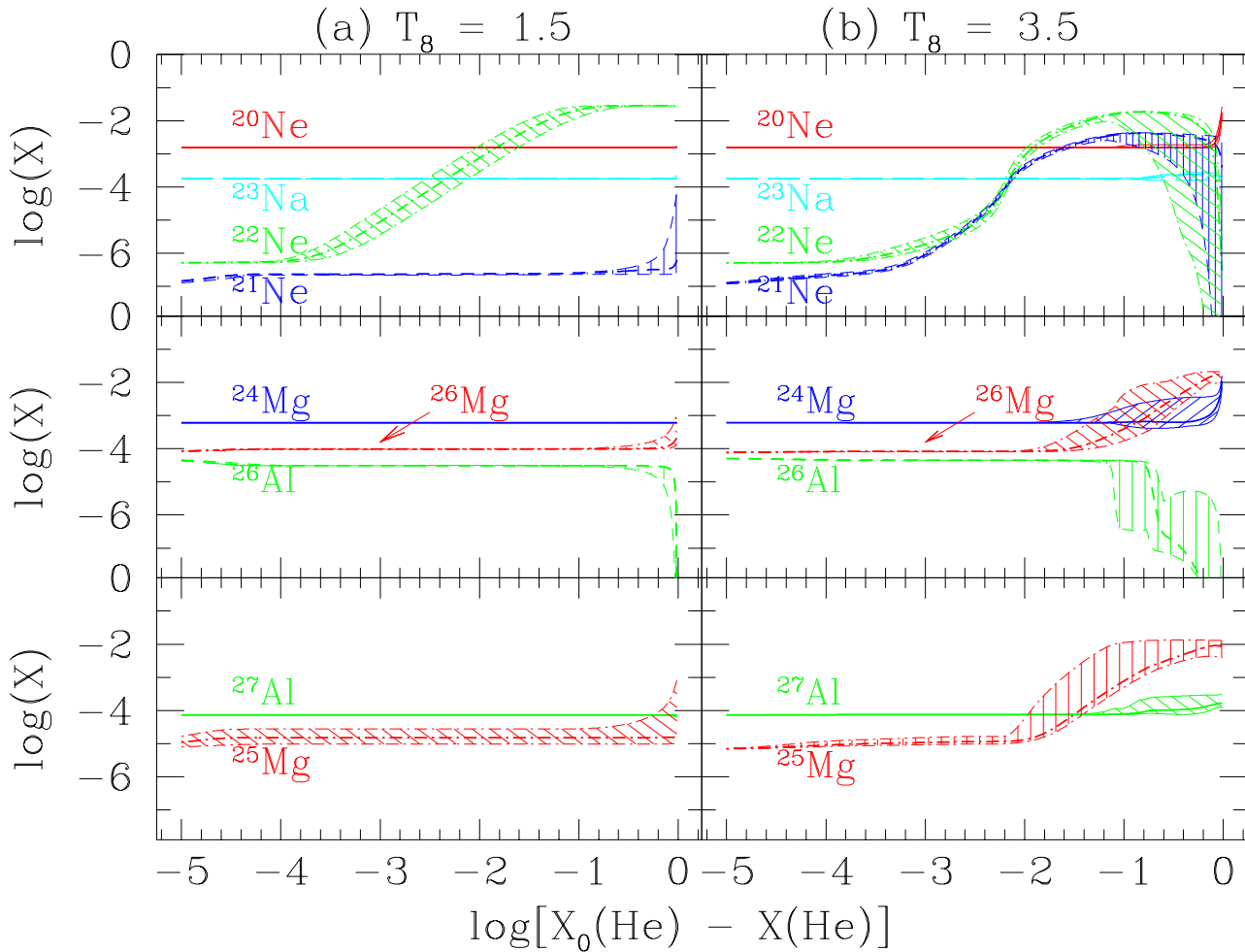


Fig. 11. Same as Fig. 10 for the nuclides from Ne to Al

abundances are smaller at higher temperature. Neutrons are also responsible for the destruction of any ^{26}Al that may survive the former H-burning episode.

The operation of $^{22}\text{Ne}(\alpha, n)^{25}\text{Mg}$ at the end of He burning leads to a non-negligible neutron irradiation which triggers a weak s-process leading to the overproduction of the $70 \lesssim A \lesssim 90$ s-nuclei. Unfortunately, the rate of $^{22}\text{Ne}(\alpha, n)^{25}\text{Mg}$ remains quite uncertain (Fig. 12), even at temperatures as high as $T_8 = 3.5$ (in this case by a factor of 25). The resulting uncertainty on the neutron density amounts to a factor of 10 (Fig. 13), while the total neutron exposure spans the range $0.1 - 0.3 \text{ mbarn}^{-1}$. Finally, the α -captures by the Ne isotopes are fast enough at temperatures $T_8 > 3$ to alter the Mg isotopic composition. This may provide a direct observational signature of the operation of the $^{22}\text{Ne}(\alpha, n)^{25}\text{Mg}$ neutron source in stars (e.g. Malaney & Lambert 1988). Large uncertainties remain, however, in these reaction rates at He-burning temperatures, except for the relatively well-determined $^{20}\text{Ne}(\alpha, \gamma)^{24}\text{Mg}$ rate.

7. Conclusions

As an aid to the confrontation between spectroscopic observations and theoretical expectations, the nucleosynthesis associated with the cold CNO, NeNa and MgAl modes of H burning, as well as with He burning, is studied with the help of the recent NACRE compilation of nuclear reaction rates. Special attention is paid to the impact on the derived abundances of the carefully evaluated uncertainties that still affect the rates of many reactions. In order to isolate this nuclear effect in an unambiguous way, a very simple constant temperature and density model is adopted.

It is shown that large spreads in the abundance predictions for several nuclides may result not only from a change in temperature, but also from nuclear physics uncertainties. This additional intricacy has to be kept in mind when trying to interpret the observations and when attempting to derive constraints on stellar models from these data.

Acknowledgements. This work has been supported in part by the European Commission under the Human Capital and Mo-

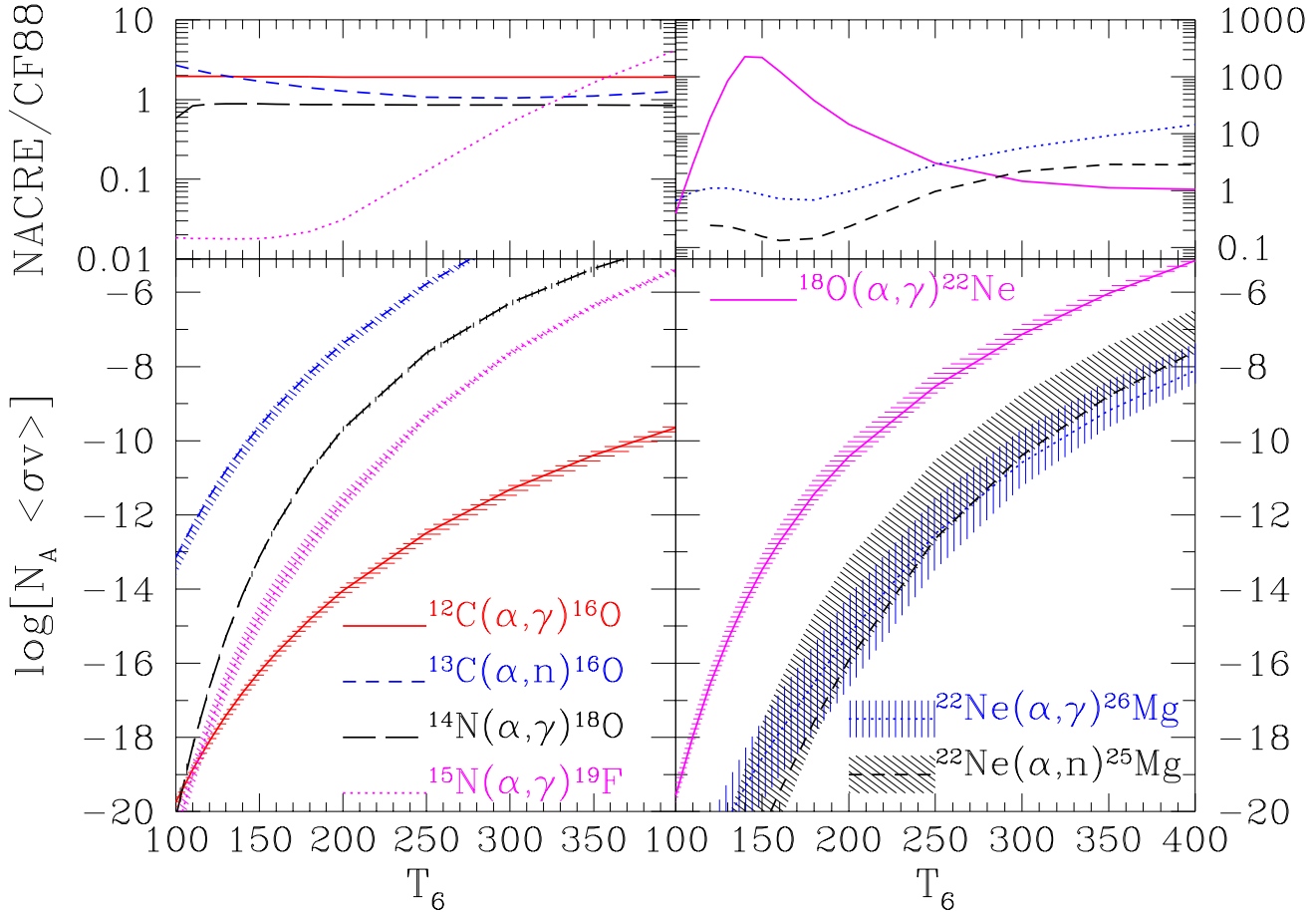


Fig. 12. Same as Fig. 4 for some α -capture reactions

bility network contract ERBCHRXT930339 and the PECO-NIS contract ERBCIPDCT940629.

References

- Anders E., Grevesse N., 1989, *Geochim. Cosmochim. Acta* 53, 197
- Angulo C., Arnould M., Rayet M., et al. (the NACRE Collaboration), 1999, *Nucl. Phys.*, to appear
- Arnould M., Mowlavi N., Champagne A., 1995. In: Noels A. et al. (eds.) *Stellar evolution: What should be done?* (32nd Liège Internat. Astrophys. Coll.). Univ. de Liège, p. 17
- Caughlan G.R., Fowler W.A., 1988, *Atomic Data and Nucl. Data Tables* 40, 283 (CF88)
- Castellani V., Degl'Innocenti S., Fiorentini G., Lissia M, Ricci B., 1997, *Phys. Rep.* 281, 309
- Coc A., Porquet M.-G., 1998, In: Arnould M. et al. (eds.) *Tours Symposium on Nuclear Physics III*, AIP Conf. Proc. 425. American Inst. Phys., p. 457
- Dearborn D.S.P., 1992, *Phys. Rep.* 210, 367
- Denissenkov P.A., Da Costa G.S., Norris J.E., Weiss A., 1998, *A&A* 333, 926
- Fowler W.A., Caughlan G.R., Zimmerman B.A., 1975, *ARA&A* 13, 69
- Goriely S., Jorissen A., Arnould M., 1989, In: Hillebrandt W., Müller E. (eds.) *Proceedings of the 5th Workshop on Nuclear Astrophysics*. Max-Planck-Institut für Astrophysik report MPA/P1, Garching bei München, p.60
- Güsten R., Ungerechts H., 1985, *A&A* 145, 241
- Huss G.R., Hutcheon I.D., Wasserburg G.J., 1997, *Geochim. Cosmochim. Acta* 61, 5117
- Heger A., 1998, Ph.D. Thesis, Technische Universität München (Max-Planck-Institut für Astrophysik MPA-1120; unpublished)
- Jorissen A., Smith V.V., Lambert D.L., 1992, *A&A* 261, 164
- Kraft R.P., Sneden C., Smith G.H., Shetrone M.D., Fulbright J., 1998, *AJ* 115, 1500
- MacPherson G.J., Davis A.M., Zinner E.K., 1995, *Meteoritics* 30, 365
- Malaney R.A., Lambert D.L., 1988, *MNRAS* 235, 695
- Meynet G., Arnould M., 1996, In: J.M. Vreux et al. (eds.) *Wolf-Rayet Stars in the Framework of Stellar Evolution* (33rd Liège Internat. Astrophys. Coll.). Univ. de Liège, p. 89
- Meynet G., Arnould M., 1999, *A&A*, submitted
- Mowlavi N., Jorissen A., Arnould M., 1996, *A&A* 311, 803
- Mowlavi N., Jorissen A., Arnould M., 1998, *A&A* 334, 153
- Prantzos N., Diehl R., 1996, *Phys.Rep.* 267, 1
- Rolfs C.E., Rodney W.S., 1988, *Cauldrons in the Cosmos*. The University of Chicago Press, Chicago

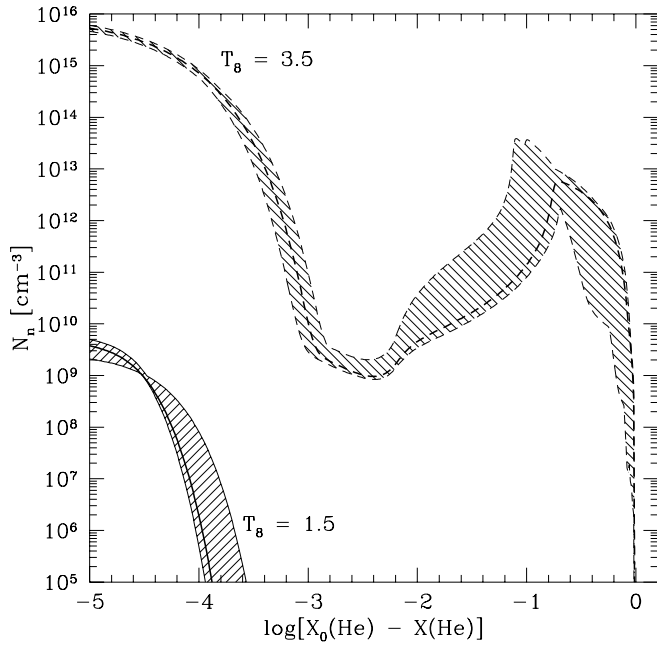


Fig. 13. Neutron density versus the amount of helium burned at $\rho = 10^4 \text{ g cm}^{-3}$ and $T_8 = 1.5$ (solid line) or $T_8 = 3.5$ (dashed line). The initial ^{13}C mass fraction is adopted equal to 10^{-4} , which is obtained at the end of the CNO cycle operating at $T_6 = 60$ and $\rho = 100 \text{ g cm}^{-3}$ (Sect. 3)

Zinner E., 1995, In: Busso M., Gallino R., Raiteri C.M. (eds.) Nuclei in the Cosmos III, AIP Conf. Proc. 327. American Inst. Phys., p. 567